

Sea level and climatic controls on turbidite occurrence for the past 26 kyr on the flank of the Gaoping Canyon off SW Taiwan



Shun-Wen Yu^{a,b}, Louis L. Tsai^a, Peter J. Talling^b, Andrew T. Lin^{c,*}, Horng-Sheng Mii^d, San-Hsiung Chung^e, Chorng-Shern Horng^f

^a Institute of Applied Geology, National Central University, Taiwan

^b National Oceanography Center, Southampton, United Kingdom

^c Department of Earth Sciences, National Central University, Taiwan

^d Department of Earth Sciences, National Taiwan Normal University, Taiwan

^e Central Geological Survey, MOEA, Taipei, Taiwan

^f Institute of Earth Sciences, Academia Sinica, Taipei, Taiwan

ARTICLE INFO

Keywords:

Taiwan
Gaoping Canyon
Turbidite
Climate change

ABSTRACT

Submarine canyons are major conduits for delivery of sediments originating from the continental margin into the deep sea. Here we analyze the effects of changing sea levels and climate (e.g. sediment supply) on the frequency of turbidites over the last 26 kyr. Our study is based on high resolution age controls for turbidites in core MD178-10-3291 from a water depth of 2070 m on the flank of the Gaoping Canyon offshore in SW Taiwan. Unlike most other submarine canyons worldwide, the head of the Gaoping Canyon has remained connected to the river mouth during the recent flooding of the continental shelf. Our results reveal that turbidity currents are less frequent during periods of sea-level lowstand. In contrast, turbidity currents have been more frequent since ~12 kyr BP, during the final stage of rising sea level and sea-level highstands. This may be the result of increased terrestrial sediment delivery due to enhanced rainfall intensity. Moreover, comparing to other source-to-sink systems, the turbidite occurrence in the flank of Gaoping Canyon through the last glacial cycle might have been more strongly influenced by climatic changes due to short sediment storage/response time.

1. Introduction

Submarine canyons are important conduits for sediment transport toward the deep sea, originating from the continental domain, as well as from slope and shelf (Weaver et al., 2000). Therefore, properly comprehending sedimentary trends and canyon architecture has major implications for geohazard evaluation, carbon cycling and sediment budgeting. Turbidity currents are amongst the major process of sediment transport within submarine canyons. These currents can transport large quantities of sediments and create some of the most significant sediment accumulations found across the world (Ingersoll et al., 2003; Talling, 2014). Moreover, these currents have the capacity to disrupt and damage telecommunication cables, pipelines, and oil and gas infrastructure (Brushci et al., 2006; Carter et al., 2012, 2014). As a result of these issues, it becomes critical to accurately comprehend the occurrences of these currents as well as the associated factors that could act as triggers to these currents.

There is a great diversity of sediment dispersal in different submarine canyons around the world, with a range of source and sink

characteristics on continental margins (Walsh and Nittrouer, 2009). The influences of sediment delivery from rivers to oceans include tectonic processes, which control the topography along the sediment dispersal system, and climate, which controls the weathering and erosion in river catchments (Allen, 2008). It is the case that, for most sediment-routing systems in the world, the submarine canyons are detached from river mouths (Liu and Lin, 2004); only in rare cases does the submarine canyon head, such as in the Gaoping Canyon head (Liu et al., 2002), reach into or very near the mouth of the river. In addition, the Gaoping sediment-routing system also represents a source-to-sink system, through which terrestrial sediments are quickly removed and transported to the deep sea by episodic gravity flows in a mountainous catchment (Sparkes et al., 2015; Selvaraj et al., 2015; Liu et al., 2016). Therefore, the river-sea system of Gaoping is an important example for studying the source, pathway, transport and fate of terrestrial material derived from mountain belts to the deep sea.

* Corresponding author at: Department of Earth Sciences, National Central University, 32001 No. 1 Chungda Road, Chungli, Taoyuan, Taiwan.
E-mail address: andrewl@ncu.edu.tw (A.T. Lin).

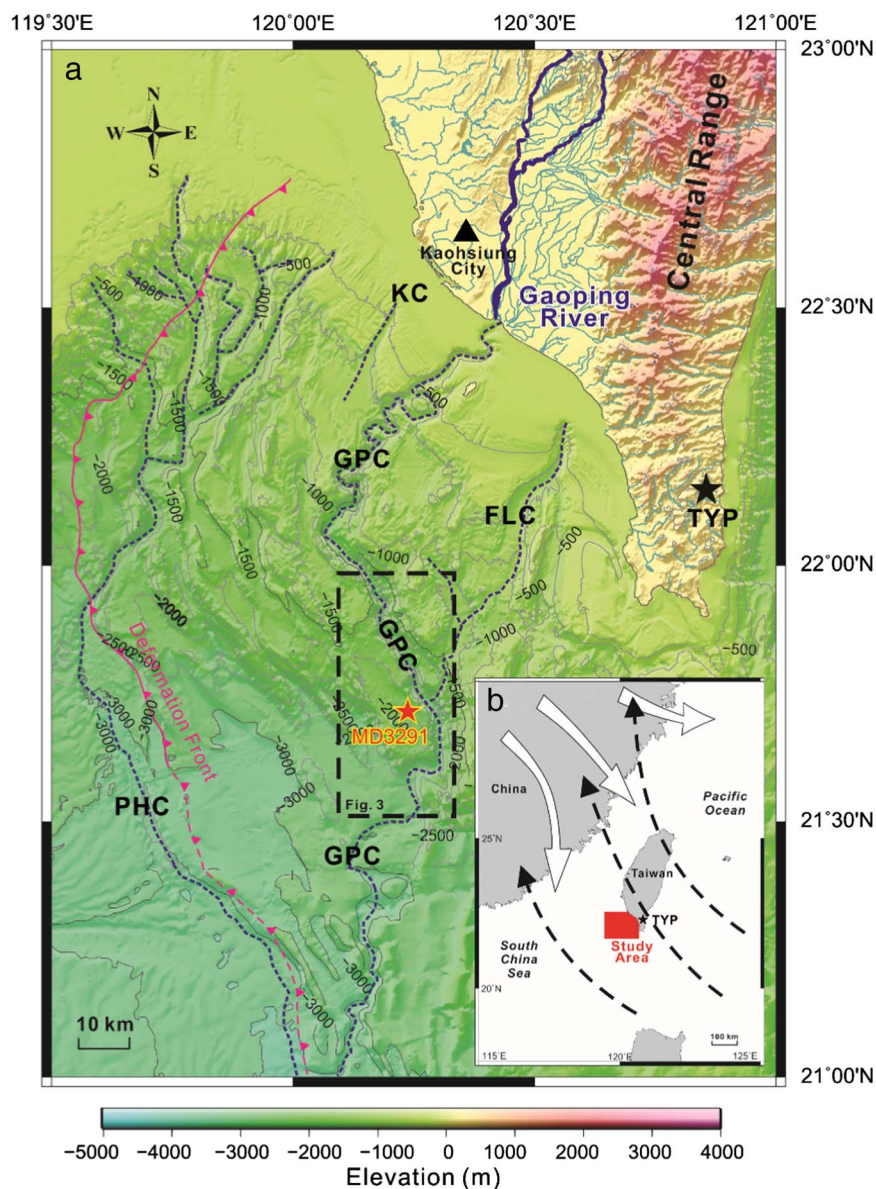


Fig. 1. (a) Seafloor bathymetry offshore SW Taiwan with the location of MD178-10-3291 (denoted as the red star). Location of deformation front is from Lin et al. (2008). FLC: Fangliao Canyon, GPC: Gaoping Canyon, KC: Kaohsiung Canyon, PHC: Penghu Canyon, TYP: Tung-Yuan Pond. (b) Map of Taiwan and its vicinity showing the paths of winter and summer monsoons, as indicated by open and dashed arrows, respectively (modified from Yang et al., 2011). Location of the study area off SW Taiwan is marked by a red rectangle.

1.1. Recent observations on turbidity currents and sedimentation in the Gaoping Canyon

The source to sink system of the Gaoping River/Shelf/Canyon situated in the southern region of Taiwan, and the areas in the vicinity (Fig. 1) constitutes a decent natural system for the assessment of the origin, paths, procedure, and ultimate outcome of sediment originating from the mountain belts in Taiwan and extending far into the South China Sea. Direct flow monitoring in the upper Gaoping Canyon was undertaken between 2000 and 2010 (Liu and Lin, 2004; Liu et al., 2002, 2004, 2006, 2009, 2012, 2013; Z. Liu et al., 2010a; J.T. Liu et al., 2010b; Hsu et al., 2014). Frequent turbidity currents have been observed in the upper canyon, and these turbidity currents typically result from river flooding, remobilisation of recently deposited flood sediments and re-suspended sediments caused by storm waves (Liu and Lin, 2004; Liu et al., 2004, 2009; Z. Liu et al., 2010a; J.T. Liu et al., 2010b), or from earthquake-triggered slope failures (Hsu et al., 2008; Liu et al., 2009; Carter et al., 2014) (Table 1). Moreover, nepheloid layers with high suspended sediment concentrations and induced by hyperpycnal turbidity currents have also been observed offshore from the Gaoping River mouth (Hsu et al., 2014) (Fig. 2).

Despite the lack of flow monitoring in the middle and lower reaches of the Gaoping Canyon, two recent submarine cable breakage events (i.e., during the 2006 Pingtung earthquake and the 2009 Morokot Typhoon) reveal that turbidity currents triggered by onshore floods and earthquakes are also important for the middle and lower reaches of the canyon (Hsu et al., 2008; Liu et al., 2012, 2013; Su et al., 2012; Carter et al., 2012; Kao et al., 2010) (Fig. 2).

1.2. Objectives of this study

Most previous studies on turbidity currents in this area have focused on modern flows and recent sedimentary processes (e.g., Carter et al., 2014; Liu et al., 2012, 2013; Su et al., 2012; Huh et al., 2009). However, the effects of millennial-scale climatic changes and glacial-to-deglacial cycles on sediment dynamics are poorly known. In this study, we reconstruct the late Quaternary turbidite history of the Gaoping Canyon flank for the past ~26 kyr, based on detailed sediment descriptions and high-resolution age models from long piston cores. We discuss the sedimentary imprints of the interplay between sea level and climatic changes, and their relative importance for triggering turbidity currents.

Table 1
Possible triggers for flow (turbidity currents) in the Gaoping Canyon.
Modified from Talling (2014).

Triggers	Type of flow produced; frequencies	Key references
Slope failure in canyon-head or canyon margins	Rapid deposition of flood sediment may lead to delayed slope failure; earthquakes may trigger multiple slope failures. Both can lead to canyon flushing events that reach deep ocean.	Hsu et al., 2008; Carter et al., 2012
Plunging hyperpycnal river flood discharge	Proposed here that these events form dilute and slow flows that deposit thin laminae. Unknown whether they can reach deep ocean	Liu et al., 2012, 2013
Large waves during storms	Wave loading may re-suspend sediments in the canyon as for canyons fed by oceanographic processes.	Liu et al., 2006, 2009, 2012

2. Regional settings of the study area

2.1. Gaoping fluvial and canyon system

Sediments from the delivery river, the Gaoping River, is around 49 Mt/yr(s) (Dadson et al., 2003), which is the largest source of sediments discharged from southwestern Taiwan (Fig. 1a). Moreover, it also delivers sediments directly into the Gaoping Canyon (Liu et al., 2002; Liu et al., 2004), making the Gaoping Canyon an important sediment

dispersal system for the northern South China Sea (Yu et al., 2009).

The Gaoping Canyon traverses the narrow Gaoping Shelf (< 10 km wide) and the broad Gaoping Slope, with the canyon head located < 1 km from the Gaoping River mouth (Fig. 1a). This canyon consists of three distinct segments along its course: an upper reach, a middle reach and a lower reach (Chiang and Yu, 2006). The upper reach has water depths ranging from 126 m to 1750 m, meanders southwesterly through the upper slope area, and is characterized by high relief. The middle reach is straight, with its thalweg made up of water depths

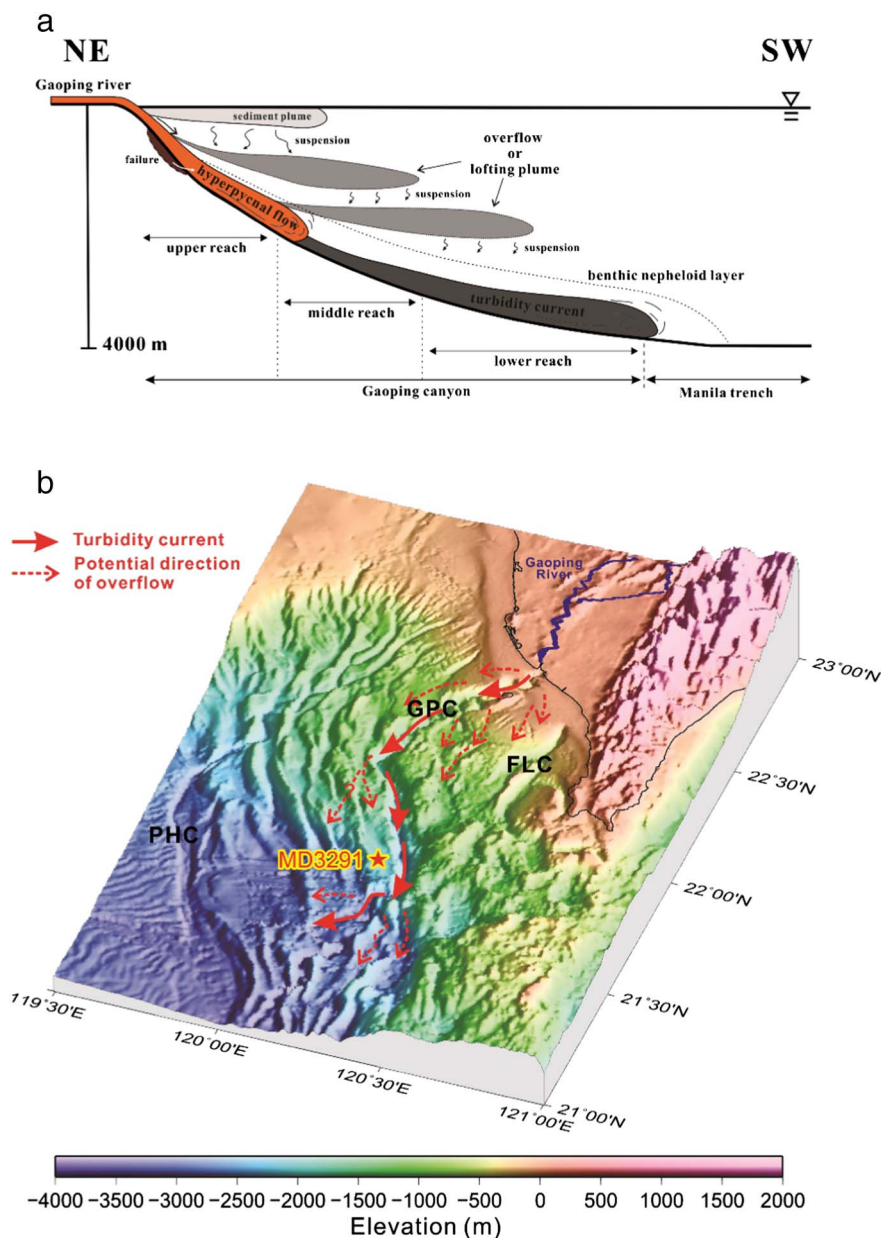


Fig. 2. (a) A schematic drawing showing possible processes of sediment delivery into the ocean/Gaoping Canyon from the Gaoping River mouth. (b) A 3D shaded relief map for onshore and offshore southern Taiwan. Arrows in and around the Gaoping Canyon system show potential flow directions and paths for turbidity currents and its associated flows. Acronyms can be found in Fig. 1.

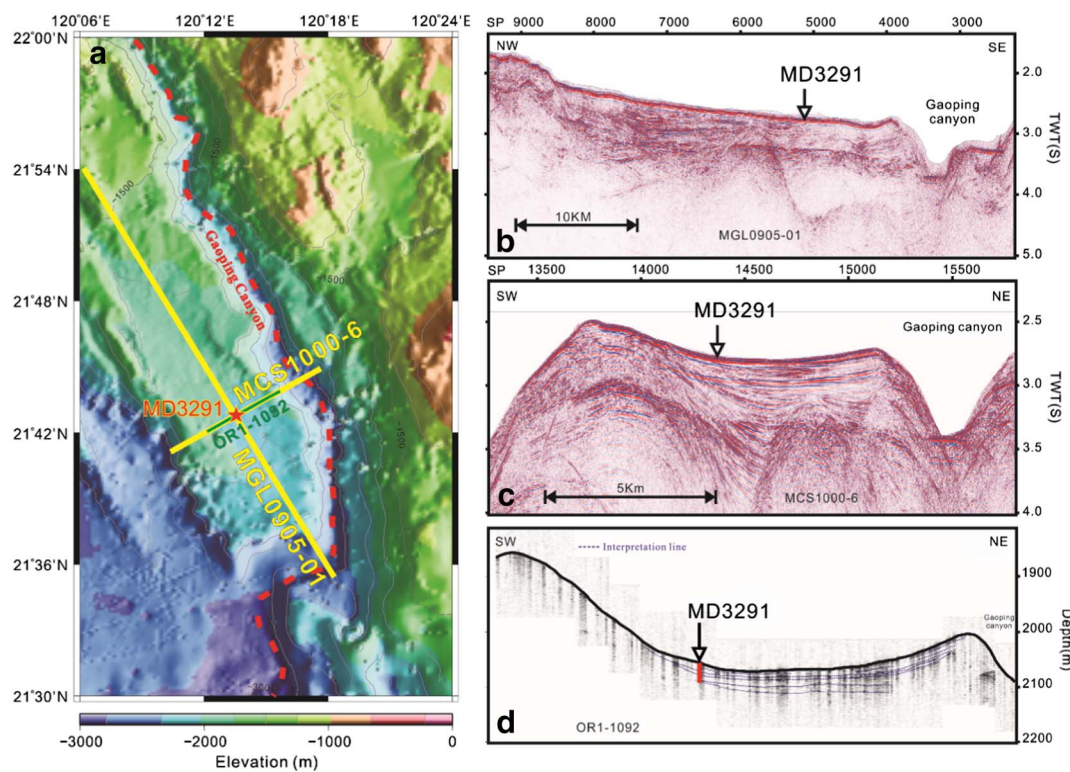


Fig. 3. (a) Shaded relief map in the vicinity of the studied core MD3291, showing the canyon thalweg and margins of the middle Gaoping Canyon segment. Seismic and CHIRP profiles crossing the MD3291 locations are also shown. (b) and (c) are the seismic profiles crossing MD3291 site in the NW-SE (MGL0905-01) and the SW-NE (MCS1000-6) directions, respectively. MGL0905-01 was acquired by using R/V Marcus G. Langseth in 2009 and MCS1000-6 was collected by using R/V Ocean Researcher I in 2012. (d) A CHIRP profile crossing MD3291 site in a SW-NE direction with interpretations (blue dotted lines).

ranging from 1750 m to 2800 m. It runs southeastwardly along an elongated escarpment and makes a sharp turn to the southwest. The relief from the canyon thalweg to flank in the middle segment is around 500–700 m. Here we study core MD178-10-3291 (abbreviated as MD3291) located on the west flank of the canyon in this middle segment (Figs. 1a, 3a).

The lower reach of the canyon meanders across the lower accretionary wedge and connects to the northern Manila Trench (Liu et al., 1993) with water depths ranging from 2800 to 3600 m. Its thalweg to levee relief is around 200–300 m. The course and morphology of the Gaoping Canyon are strongly controlled by thrusting and folding processes in the accretionary wedge (Chiang and Yu, 2006), leading to two prominent sharp bends in the canyon course.

2.2. Climate in southern Taiwan

Taiwan and its surrounding region are greatly influenced by the monsoon of East Asia (Fig. 1b). Amongst the most critical climate features of the island is the Pacific typhoon systems, which leads to the creation of tropical cyclones during the mid-summer to early-autumn each year (Chen et al., 2007). Between 1949 and 2009, 255 typhoons passed through Taiwan, an average of approximately 4 typhoons per year (Liu et al., 2013). Periodical rainfall as a result of tropical cyclones leads to increased sediment discharge and run-off in the river systems of Taiwan (Chen et al., 2006; Galewsky et al., 2006; Goldsmith et al., 2008). In terms of temperature, southern Taiwan has averaged seasonal variations of 20.5 °C to 28.0 °C since 1897. Average monthly rainfall spans between 20.3 mm to 510.1 mm, demonstrating a significant trend for high and low rain periods during the summer and winter seasons, respectively (Wang et al., 1994). Enhanced precipitation resulting from tropical cyclones that occur in summer and early fall contributes > 85% of the annual rainfall in southern Taiwan (Wang et al., 1994).

Variations in the post-glacial climates and vegetation in South

Taiwan were assessed through pollen content extracted from sediments collected from the Tung-Yuan Pond (TYP), Taiwan (Fig. 1a) by Lee and Liew (2010) and Lee et al. (2010). Their research concluded that the climate of Taiwan (the southern region, in particular) has followed the solar-radiation since the last glaciation. It was cold during the Last Glacial Maximum (LGM) and the early deglaciation, and warmed around the later deglaciation period, reaching its highest temperature during the Holocene Thermal Optimum (HTO), before once again cooling down during the late Holocene. Paleo-precipitation derived from organic proxies assessed through the TYP sediment core demonstrates that variations in the rainfall frequency are most likely reactions to the changing monsoon strength in the region (Yang et al., 2011). The frequency and intensity of rainfall increased in South Taiwan in four major phases: deglaciation (~17.2 to ~13 kyr BP), early Holocene (~10.6 to ~8.6 kyr BP), the middle Holocene Thermal Optimum (~7.7 to ~5 kyr BP) and the late Holocene (~4.2 to ~2 kyr BP). It appears that the middle Holocene observed the most stable and increased rainfall.

3. Materials and methods

3.1. Sediment core

The studied core, MD3291, was acquired during a phase of a ‘gas hydrate study’ project that was funded by the Central Geological Survey, Taiwan in 2010, utilizing the R/V Marion Dufresne. The core is situated over the west bank and lower slope of the Gaoping Canyon (Figs. 1a and 3a). Compared with the depth of the thalweg, the core is located roughly 600 m higher (Fig. 3a). Chirp/Seismic profiles across the position of our studied core reveal that strata in the west bank and the lower slope of the Gaoping Canyon are nearly continuous and horizontal in the NW-SE direction (Fig. 3b), and in the NE-SW direction, the strata reveal a “sediment wedge”, thinning away from the canyon

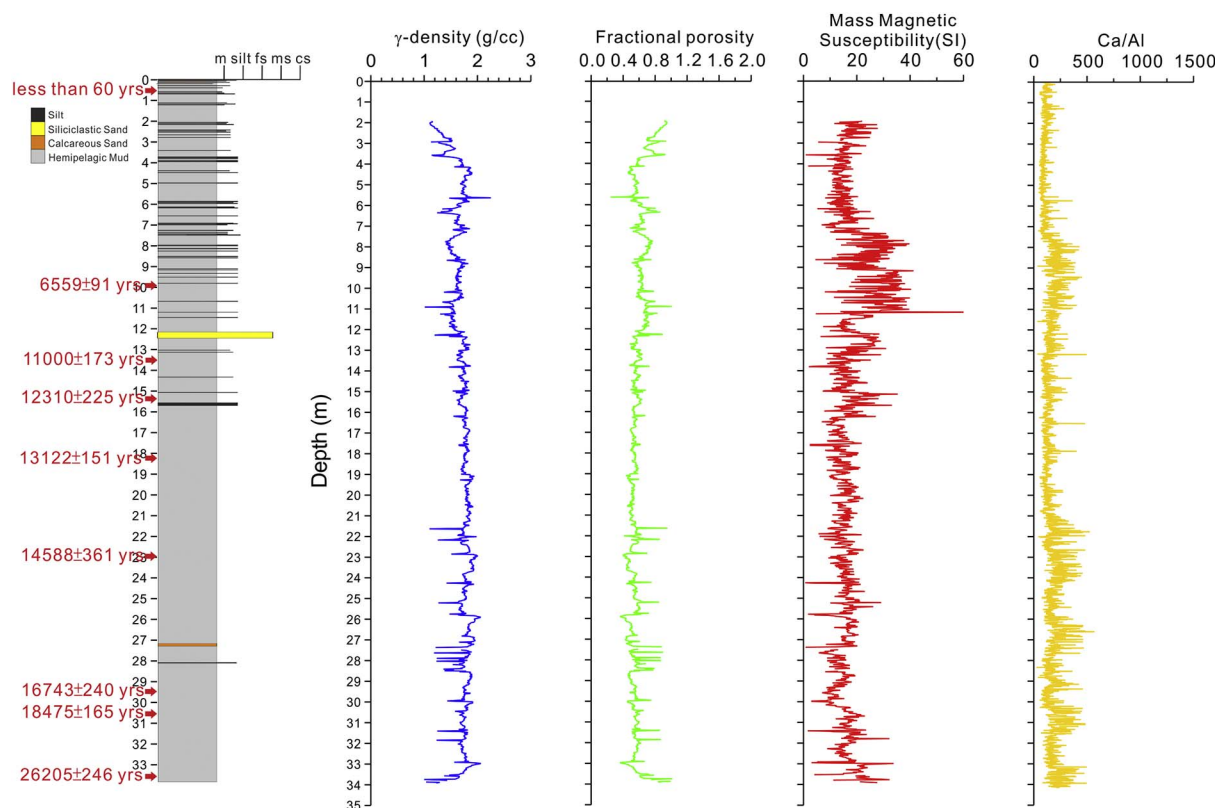


Fig. 4. Lithological descriptions, dated ages, and petrophysical characteristics (density, porosity and magnetic susceptibility) and geochemical data from MSCL and ITRAX XRF core scanner for core MD3291.

(Fig. 3c and d).

This core was logged with 1 cm resolution for basic petrophysical (i.e., magnetic susceptibility (SI), γ -density (g/cm^3), fractional porosity) and geochemical characteristics by using a Geotek Multi-Sensor Core Logger (MSCL) and an ITRAX XRF (X-Ray Fluorescence) core scanner (Fig. 4).

3.2. Identification of turbidites and hemipelagites

In order to develop age models and determine recurrence intervals for turbidity currents, differentiating turbidites from background hemipelagic sediments is vital. We tried to differentiate these deposits by grain-size analyses, visual logging, and X-ray images. However, the results of grain-size analyses, which were performed on pretreated sediments (carbonates were removed by using 10% hydrochloride (HCl) and carbonate-free samples were treated with 15% hydrogen peroxide (H_2O_2) for 1–2 days to remove organic matter) with the laser diffraction particle size analyzer (Beckman Coulter LS13 320) for every 1 cm-thick sediment. The grain size results and laminations shown on X-ray images do not correlate very well (Fig. 5a). This is due to the studied turbidites are generally < 1 cm and our grain-size sampling interval is 1 cm interval. Therefore, the nature of thin turbidite bed precludes us from carrying out grain size analysis for a turbidite bed to examine its vertical grain size variations. In other words, the main methods to differentiate turbidites from background hemipelagic sediments in this study are visual logging and X-ray images.

Criteria used to identify turbidites in cores are lithology and sedimentary structures. Hemipelagic sediments usually consist of homogeneous grey clay deposits and typically contain randomly dispersed foraminifera giving a pitted surface texture. In contrast, turbidites are characterized by mm to cm-thick, mainly composed of very fine to medium-grained sands with commonly erosional bases. In this paper, the thickness definition follows Tombo et al.'s (2015) terms. We use the

term of laminae to describe layers < 1 mm, and bed for those > 1 mm.

On X-ray imagery (Fig. 5), the transition from dense (dark) lower contacts to light (grey) top of beds, is associated with the typical fining-up trend of turbidites (Bouma, 1962; Stow and Piper, 1984). X-ray images have also been used to precisely locate the hemipelagic intervals sampled for forams for ^{14}C dating and mineral analyses.

3.3. Mineral analyses for turbidites on MD3291

In order to assess the potential origin of turbidites for the studied core, distinguishing the mineralogy for coarser grained sediments in turbidites was conducted. Because most turbidites in MD3291 are very thin (< 0.5 cm) and composed of silts to very fine-grained sediments, it is difficult to analyze the mineral composition of the coarser grained sediments in turbidites from thin sections under a polarised microscope. Hence, we estimated the mineral composition of each turbidite layer under stereo-microscopes and checked if there are slate fragments, which must be derived from Taiwan.

3.4. Age model

3.4.1. AMS ^{14}C dating

Over 300 specimens of planktonic foraminifera, including the *Orbulina universa* and *Globigerinoides* spp., were picked with criterion of a size fraction > 250 μm for eight intervals hosting adequate foraminifera. For the sample at depth 50–52 cm, a large piece of plant fragment was picked for dating. The collected samples were sent to Beta Analytic Inc. for AMS ^{14}C dating. The reported AMS ^{14}C ages were converted to “calendar ages” using the CALIB 7 Program (<http://radiocarbon.pa.qub.ac.uk/calib/>). For the conversion, we adopted a $\Delta R = 0$ (the local difference in reservoir age from 400 years; Bard, 1988). The calibrated ages were then converted into years BP (i.e., before AD1950, Table 2).

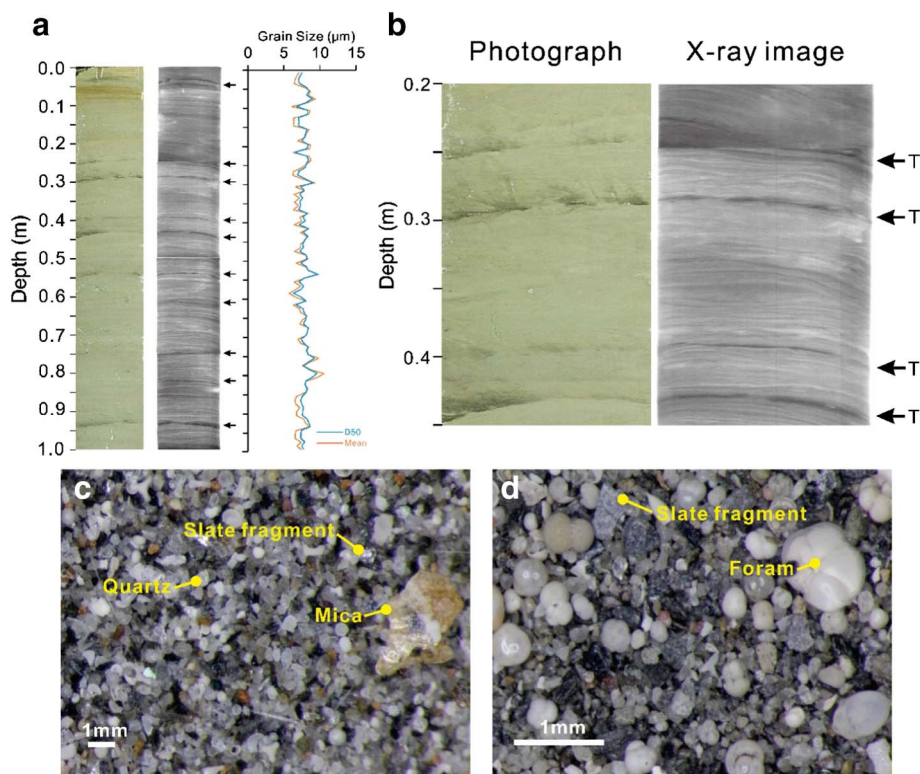


Fig. 5. (a) Sedimentary characteristics and the variations of sediment grain size (D50 represents median and mean represents average grain size) at MD3291 core. The core depth is from 0 to 1 m. Thin turbidite layers (arrowed) at 0–0.05 m, 0.25 m, 0.3 m, 0.4 m, 0.44 m, 0.54 m, 0.62 m, 0.75 m, 0.82 m and 0.93 m. (b) Sedimentary characteristics of turbidites for an enlarged part of the MD3291 core (0.2–0.45 m depth) shown by photo and X-ray images (T represents turbidite). Mineralogy of thin layer turbidites (c) at 2.71 m and thick layer turbidite (d) at 13.85 m in MD3291. Note that both turbidite layers contain rich slate fragments.

3.4.2. Oxygen isotope

Oxygen isotope stratigraphy ($\delta^{18}\text{O}$) for MD3291 core was established through planktonic foraminifera of *Neogloboquadrina dutertrei*. Around 3 to 5 specimens of *N. dutertrei*, ranging 250 μm to 300 μm in size, were picked and cleaned with due attention and caution. Picked foraminifera were then put in an ultrasonic bath with methanol for 5 times. Following the removal of the methanol relict, we immersed all specimens in a NaOCl solution for at least 24 h. Subsequently, DD-water was utilized to clean the foraminiferal shells. After the cleansing process, the foraminifera were dried overnight in an oven at 50 $^{\circ}\text{C}$. The Micromass IsoPrime isotope ratio mass spectrometer, housed in the Stable Isotope Laboratory, National Taiwan Normal University, was utilized for our samples, and precisions for oxygen isotope values are 0.05‰ (n = 532).

3.5. Turbidite recurrence intervals

Using the age model to estimate the emplacement ages for each turbidite allows us to calculate recurrence intervals. Here we assume the erosional thickness below turbidite layers at MD3291 is negligible. We define the recurrence interval of a turbidite layer as the length of time since the turbidite that preceded it (e.g., Clare et al., 2014, 2015). Where hemipelagic age model cannot be constructed in details, we calculate the recurrence interval by dividing the length of time by number of turbidite layers to yield an “averaged recurrence interval”.

4. Results

4.1. Sedimentary characteristics and mineral compositions

Sediments of MD3291 consist of hemipelagic muds, frequent lamina

Table 2
A list of AMS Carbon-14 dating for MD3291Core.

No.	BETA no.	Depth (m)	Conventional age (BP yr)	2 σ cal age (BP yr)	Materials
MD3291	351526	0.52–0.53	–	The last 60 yr	Plant fragment
MD3291	377506	9.92–9.96	6130 \pm 30	6559 \pm 91	<i>Orbulina universa</i> <i>Globigerinoides</i> spp.
MD3291	348537	13.51–13.55	10,030 \pm 40	11,000 \pm 173	<i>Orbulina universa</i> <i>Globigerinoides</i> spp.
MD3291	348536	15.42–15.46	10,830 \pm 50	12,310 \pm 225	<i>Orbulina universa</i> <i>Globigerinoides</i> spp.
MD3291	348538	18.23–18.27	11,640 \pm 50	13,122 \pm 151	<i>Orbulina universa</i> <i>Globigerinoides</i> spp.
MD3291	358257	22.97–23.01	12,850 \pm 50	14,588 \pm 361	<i>Orbulina universa</i> <i>Globigerinoides</i> spp.
MD3291	358256	29.51–29.55	14,240 \pm 50	16,743 \pm 240	<i>Orbulina universa</i> <i>Globigerinoides</i> spp.
MD3291	358258	30.49–30.53	15,610 \pm 60	18,475 \pm 165	<i>Orbulina universa</i> <i>Globigerinoides</i> spp.
MD3291	373603	33.60–33.64	22,380 \pm 90	26,205 \pm 246	<i>Orbulina universa</i> <i>Globigerinoides</i> spp.

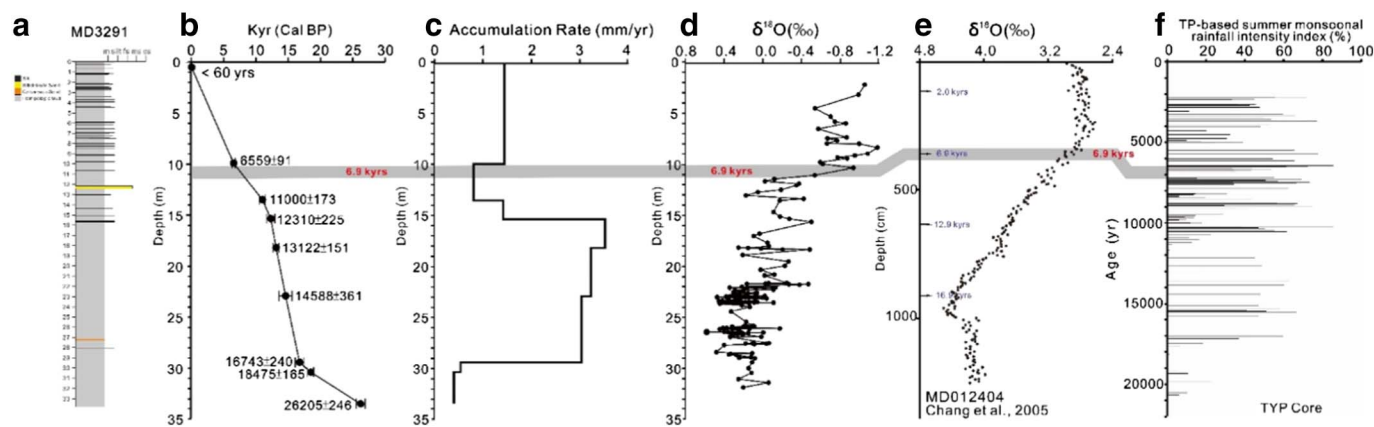


Fig. 6. Age model and oxygen isotope stratigraphy of MD3291 core offshore SW Taiwan. (a) Graphic sedimentologic logs for MD3291. (b) Age (AMS ^{14}C dating) and depth relationship. (c) Variations of sediment accumulation rate through time. (d) Oxygen isotope stratigraphy at MD3291. (e) Oxygen isotope stratigraphy and age dates of MD012404 core of Chang et al. (2005) in the southern Okinawa Trough offshore NE Taiwan. (f) Rainfall intensity index (%) for the TYP core (Yang et al., 2011). The consistency of age dates and corresponding variations of oxygen isotope curve suggests that the age model for MD3291 is robust. The thick grey line is the correlated time line for ~ 6.9 kyr.

and thin silt beds (< 1 cm), and occasional thick sand beds (> 1 cm) (Fig. 4). The length of MD3291 core is 34.09 m, and the lower part of the core (~ 13.50 – 34.09 m) consists of homogenous hemipelagic muds with only two thick (> 2 cm thick) fine-grained sand beds (Fig. 4). The hemipelagite is grey in color and often contains randomly dispersed foraminifera. The upper part of the core (~ 0 to 13.50 m) is dominated by grey muds and silt interlayers (usually < 1 cm thick) with one thick (~ 5 cm thick) medium-grained sand bed (13.80–13.85 m). The silt beds show parallel laminations and weak normal grading and parallel laminations (Fig. 5b), and the medium-grained sand bed shows obvious normal grading. Moreover, the major coarser-grained mineral compositions of the thin silt beds are quartz, slate fragments, mica and a few fossils (Fig. 5c); whereas the thicker sand beds are composed mostly of fossils, slate fragments and quartz (Fig. 5d).

4.2. Age model and sedimentation rate

The age model for core MD3291 is established by 9 AMS ^{14}C age dates as summarized in Table 2 and shown in Fig. 6a (between 10 m and 0.5 m, we have only one ^{14}C dating age at 9.92–9.96 m interval. This is because that the sediments between 10 and 0.5 m are lack of *Orbulina universa* and *Globigerinoides* spp. for dating). The plant fragment at 51 cm core depth reveals more ^{14}C existing in this sample than modern (1950 CE) reference standard. The excessive radiocarbon context (^{14}C) could be derived from the thermonuclear bombing during the 1960s (e.g. Nydal and Lövseth, 1965). In simpler terms, sediments found above 51 cm in the core have been deposited since following nuclear testing in 1960s CE. This result brings an important information to us that the modern sediments at the seafloor is also retrieved and the core is not under-sampled as commonly occurred in many Calypso piston coring system.

The 9 dated ages show a progressive younging upward trend, indicating the age dates are consistent. The age model is further validated by oxygen isotope stratigraphy (Fig. 6c) measured from the planktonic foraminifera of *N. dutertrei*. The measured oxygen-isotope trend is correlatable to global isotope trends, particularly the trend observed at MD012404 located in the Okinawa Trough (e.g., Chang et al., 2005) (Fig. 6d). The consistency of age dates and corresponding variations of oxygen isotope do reflect that the employed age framework for MD3291 is effective for its purpose.

Based on the age model of MD3291, one can observe that the rate of sediment accumulation (constituting hemipelagites and turbidites) is relatively low, about 0.41 mm/yr, during glacial and early deglacial stages (from ~ 26 to 16.7 kyr). Between ~ 16.7 to 12 kyr, an increase can be observed with the rate of accumulation at around 3 mm/yr

(Fig. 6b), and during the following ~ 12 kyr, the rate of accumulation slightly decreased to ~ 1.5 mm/yr. Generally, the accumulation rate during interglacial periods is roughly five times faster than the rate during the glacial stage.

4.3. Variations of turbidite recurrence intervals and thickness at MD3291

By dividing the number of turbidite layers with the time interval, we are able to calculate an average recurrence for turbidites in different periods (Table 3). Earlier than ~ 12 kyr BP, turbidity currents were rather rare, with averaged recurrence intervals of 1275 yrs (during 16.7 to 18.5 kyr BP) and 1465 yrs (during ~ 12 to 13.5 kyr BP), respectively (Table 3). However, during the following ~ 12 kyr BP, the average turbidite recurrence intervals became much shorter, with averaged recurrence intervals in the selected dating intervals being < 700 yrs. The frequency of currents has increased rather significantly since ~ 12 kyr BP.

The thickness of turbidite “bed” ranges from 0.1 to 10 cm and the average thickness for turbidites in different periods were shown in Table 3. Overall, the thickness of turbidites gradually decreases from stages of rising sea level to sea-level highstands.

5. Discussion

5.1. Turbidites on the flank of Gaoping Canyon

Turbidites in MD3291 core consist of frequent thin silt beds (< 1 cm) and occasional thick sand beds (> 1 cm) (Fig. 4). The thin silt beds show parallel laminations and weak normal grading (Fig. 5a), and the major coarser-grained mineral compositions of these thin turbidite beds are quartz, slate fragments, mica and a few fossils (Fig. 5c). The

Table 3
Average turbidite recurrence interval for each dated interval in MD3291.

Interval (yr to yr BP)	Number of turbidite layers	Average recurrence interval (yr)	Average thickness of turbidite layers (cm)
0–6559	46	139.5	0.1
6559–11,000	11	403.3	0.9
11,000–12,310	2	632.5	0.1
12,310–13,122	1	1465	2.2
13,122–14,588	0	–	–
14,588–16,743	2	1275	1.4
16,743–18,475	0	–	–
18,475–26,205	0	–	–

thick and medium-grained sand beds show obvious normal grading and comprise mainly of fossils, slate fragments and quartz (Fig. 5d). The medium-grained sands are composed of abundant reworked fossils, which may indicate that these thick beds have been originated from seabed failures from the nearby shelf or upper slope. Moreover, the thin silt beds enriched in terrestrial materials, which are similar to hyperpycnal turbidites seen in lakes and reservoirs (e.g., Lambert and Hsu, 1979; Umeda et al., 2006; Gilbert et al., 2006; Crookshanks and Gilbert, 2008). The nature of thin beds observed in lakes and reservoirs may result from dilute sediment concentrations and slow aggradation rates (Talling, 2014), and the vertical textural trend showing a normal grading from fine sands to mud can be explained by turbulent turbidity currents from suspended-load fallouts (Stevenson et al., 2014). Hence, considering the stratal characteristics of the study area (thinning away from the canyon) and the thickness and sedimentary structures of these silt layers, we interpret that the agents for delivering silt-size grains to this canyon flank are overbanking turbulent flows or nepheloid suspensions from the upper slope.

5.2. Potential effects of varying accumulation rates in the Gaoping Canyon

A lower rate of sedimentation was observed, ~ 0.41 mm/yr, since ~ 26 to 16.7 kyr in the flank of the Gaoping Canyon, and higher accumulation rate during rising sea level (from ~ 16.7 to 12 kyr) and highstand of sea level (since ~ 6000 kyr) with the accumulation rate ranging from ~ 1 to 3.5 mm/yr and nominal accumulation rate of 2.4 mm/yr, which is about 6 times faster than that during the sea-level lowstand stage (Fig. 6). As assessed by previous models, a major supply of sediments toward the deep sea would occur during periods of sea-level lowstands and transgressions (e.g., Vorren et al., 1998; Weaver et al., 2000; Ducassou et al., 2009; Lebreiro et al., 2009; Bourget et al., 2011; Tombo et al., 2015); nonetheless, results from this study reveal that major sediment supply and deposition within the Gaoping canyon region have occurred primarily during periods of transgression and sea-level highstand while reduced sediment supply and deposition during sea-level lowstand (i.e. during LGM). This feature does not fit the classical sequence stratigraphic models (e.g., Vorren et al., 1998; Weaver et al., 2000; Ducassou et al., 2009; Lebreiro et al., 2009; Bourget et al., 2011; Tombo et al., 2015) well.

There is a possibility that the increased rate of sedimentation during rising and highstand of sea level is due to re-accumulation of sediments from re-suspension of shallower seafloor sediments rather than from river inputs. However, the Gaoping Canyon is unusual as the canyon head is located close (< 1 km) to the river mouth during a full eustatic cycle. Most other canyon heads have been separated from river mouths by the Holocene rising sea levels. Therefore, variations of terrestrial sediment flux at the head of the Gaoping Canyon are relatively unaffected by sea-level changes, and the sediment flux would depend more fully on changes in precipitation in southern Taiwan (Chen et al., 2006; Galewsky et al., 2006; Goldsmith et al., 2008). Moreover, as has been established by a study on lake sediments in southern Taiwan (Yang et al., 2011), rainfall intensity and the strength of summer monsoons in Taiwan has increased over the last ~ 16.7 kyr BP, which is correlatable to periods of increased sediment accumulation in the flank of Gaoping Canyon. This prompts us to interpret that the increases in rainfall intensity and summer monsoons have been the major causes of increased sediment supply to the Gaoping Canyon area since ~ 16.7 kyr BP (Fig. 6).

In such a case, it is necessary to explain why the accumulation rate decremented in the following ~ 12 kyr BP, during which rainfall levels increased in intensity. One of possible reasons behind this could be attributed to the flooding of the Gaoping Shelf after ~ 12 kyr BP, and since then the Gaoping Canyon head has become detached from the Gaoping River mouth, which has mitigated the accumulation rate in the lower Gaoping slope. However, increasing fluvial discharge could facilitate canyon headward erosion as a result of the trapped sediments

collapsing at the canyon head and make the canyon connection keep pace with rises in sea level (Mauffrey et al., 2017). Hence, the speculation for the Gaoping Canyon head has become detached from the Gaoping River mouth may not be valid. Alternatively, the morphological change of upper canyon may also lead to varying sedimentation rate. The studied age interval is from ~ 26 kyr to present and this short time interval is unlikely to have significant morphological change for this deeply incised canyon course as previous studies do not report any morphological changes of the upper canyon since the LGM (Chiang and Yu, 2008; Yu et al., 2009). Another potential interpretation for decreased accumulation rate in MD3291 is due to partial erosion by turbidity currents as there have been more turbidity currents since ~ 12 kyr BP as seen at the MD3291 site.

5.3. Controls of climatic changes on turbidite records in the Gaoping Canyon

Triggers for turbidity currents may include (a) earthquake shaking, (b) volcanic explosions, (c) tsunami, (d) subaerial landslides into the marine environment, (e) storm wave loading, and (f) hyperpycnal flows (Piper and Normark, 2009; Goldfinger et al., 2008). In addition, oceanic circulations may also play a role in re-distributing the river-derived marine sediments and triggering the turbidity currents (Bernhardt et al., 2016). There is a possibility that oceanic circulations may change during eustatic sea level fluctuations, and the change of oceanic circulations may lead to change of the frequency of turbidity currents. Until now, we haven't had enough evidence to evaluate this scenario in the Gaoping Canyon. However, recent observations (Hsu et al., 2008; Liu et al., 2012, 2013; Su et al., 2012; Carter et al., 2012, 2014; Kao et al., 2010) pointed out that the failure of slopes, earthquakes, storm-induced waves and hyperpycnal flows are the major triggers for turbidity currents within the Gaoping Canyon. In this context, we tend to interpret the origin of turbidity currents is mainly governed by climatic and tectono-morphologic conditions.

Fig. 7 depicts the correlation between the MD3291 core with changes in the eustatic sea levels (Lambeck et al., 2014), landslide records in the upstream of the Gaoping River catchment in southern Taiwan and the Cho-shui River catchment in central Taiwan (Hsieh and Chyi, 2010), rainfall intensity (Yang et al., 2011) and spore occurrences (Lee and Liew, 2010) since the last LGM. This figure shows almost synchronous onset of rapid accumulation at MD3291 site and enhanced rain intensity onshore in southern Taiwan at the TYP core site (Yang et al., 2011) and increasing numbers of onshore landslides in central and southern Taiwan (Hsieh and Chyi, 2010). This correlation indicates the increasing frequency of turbidity currents is correlative to humid and warm climates, as revealed by spore and pollen records (Lee and Liew, 2010) and the increased intensity of rainfall (Yang et al., 2011). The humid and warm climate since ~ 12 kyr BP may have enhanced weathering processes and contributed to the formation of loose deposits in the Gaoping River catchment area (Hsieh and Chyi, 2010). Additionally, the enhanced rainfall intensity since ~ 12 kyr BP likely facilitated sediment delivery. Thus, the increased frequency of turbidity currents in the flank of Gaoping Canyon since ~ 12 kyr BP could be attributed to increasing hyperpycnal turbidity-current events resulting from enhanced onshore rainfall intensity.

5.4. Comparison with other turbidite systems

Compared to other source-to-sink systems, the turbidity-current activities in Gaoping might have been more strongly influenced by climatic changes. The Rhone turbidite system is the largest sedimentary body in the western Mediterranean Sea and is fed by inputs mainly originating from the Rhone River. The deep-sea fan is connected to a relatively large continental shelf of 50–70 km wide through the Petit Rhone Canyon, and the maximum thickness of the sedimentary series deposited by the fan is about 3600 m (Droz and Bellaiche, 1985). The

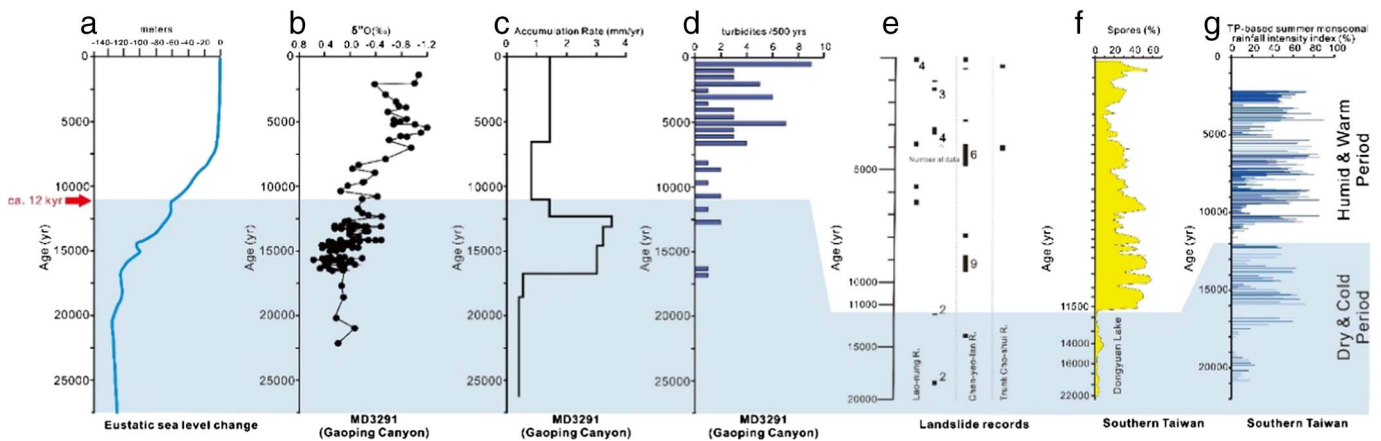


Fig. 7. Correlation of MD3291 cores to eustatic sea-levels (modified from Lambeck et al., 2014) (a), oxygen isotope stratigraphy (b), rate of sediment accumulation (c), frequency of turbidites (turbidite layers/500 yr) (d), onshore landslide records in the catchments of the Gaoping River and the Cho-shui River (Hsieh and Chyi, 2010). Data is represented as 10 calibrated range and the number is the amounts of ^{14}C datings Lao-nung River lies in the catchment of the Gaoping River in southern Taiwan and the rest of rivers (i.e., Chen-yeo-lan River and the Trunk Cho-shui River) lies in the catchment of the Cho-shui River (e), spore abundance at TYP (Lee and Liew, 2010) (f), and rainfall intensity variations at TYP (Yang et al., 2011) (g).

Table 4

Associated geomorphic characters and controlling factors in different source-to-sink systems.

Source-to-sink systems	River drainage area (km ²)	Shelf width (km)	Distance from canyon head to river mouth (km)	Controlling factors for turbidite occurrence
Gaoping system	3257 ^a	< 10	< 1	Climate (this study)
Ganges-Brahmaputra system	1,830,000 ^a	30*	~150	Complex (climate, sea level, intrinsic forcings etc.) (Fournier et al., 2016)
Rhone system	97,800 ^b	50–70	~46	Sea level (Tombo et al., 2015)

* The distance of canyon head to delta plain.

^a Data from Milliman and Syvitski (1992).

^b Data from Poit et al. (2002).

growth of the fan started during the Pliocene (5 Ma) (dos Reis et al., 2005), and since the Last Glacial Maximum (LGM) (~20 kyr BP) to the present, frequent deposition of turbidites occurred during the LGM period (sea-level lowstand). The cessation of turbidite activity occurred after the early Holocene (sea-level rise and highstand) (Tombo et al., 2015). This turbidite system is strongly influenced by sea level changes (when shelves were immersed during periods of sea level rise and highstand, the riverine sediments were trapped on shelves, and thus turbidite systems became starved). As a result of the absence of a continental shelf, the Gaoping Canyon was able to deliver more complete and continuous sedimentary records to the deep-marine environments through the last glacial cycle.

The Bengal fan is the world's largest fan system, and the SoNG (Swath of No Ground) submarine canyon represents the main connection between the sediment source and the Bengal fan (Curry et al., 2003). The SoNG deeply incises into the shelf, and thus the head of the canyon is located ~150 km from the modern river mouths of the Ganges and Brahmaputra Rivers and only ~30 km from the delta plain. Despite the fact that the Gaoping and Ganges-Brahmaputra turbidite systems are both associated with shelf-incised canyons, the forcing parameters for turbidite depositions between these two turbidite systems are different. The Active Channel in the Bengal fan was initiated around 14.5 kyr BP due to increased precipitation, which was related to an intensified Indo-Asian monsoon (Weber et al., 1997). At around 9.2 kyr BP, the sedimentation rate declined abruptly in the Active Channel as a result of a rise in sea level (Fournier et al., 2016). After ~9.2 kyr BP, turbidity-current activity is still recorded but it becomes irregular. Weakening of the Indo-Asian monsoon, stabilisation of the sea level, and intrinsic forcings as initiation of the delta and river routing impacted on turbidite activity; moreover, the anthropogenic impact is also a hypothesis to explain forcing of turbidite activity during

the last 2.5 kyr BP (Fournier et al., 2016). In other words, climatic factors do not appear to be the only predominant forcing on the establishment of the Bengal fan during the Holocene. On the flank of the Gaoping Canyon, the increased turbidite occurrence mostly reflects a period with a warm and humid climate (from ~12 kyr BP to the present) coupled with the destabilisation of mountain slopes. Besides the site-specific climate influences, the causes of the difference between the Ganges-Brahmaputra and Gaoping turbidite systems may be attributed to the difference in sediment storage/response time (Blum and Hattier-Womack, 2009) as results of: (1) the Gaoping drainage system is smaller than that of the Ganges-Brahmaputra drainage systems (Tables 4), (2) the Gaoping Canyon head is directly connected to the river mouth.

6. Conclusions

This is the first study to reconstruct the turbidite history on the flank of the Gaoping Canyon over the past ~26 kyr. Our results suggest that, during the period of sea-level lowstand (between ~26 to 16.7 kyr BP), turbidity currents in the Gaoping Canyon were scarce, and no overspill deposits are observed on the canyon flank. This is most likely due to weak onshore rainfall intensity which is likely to have delivered less terrestrial sediments into the canyon. Since ~12 kyr BP, turbidity currents in the Gaoping Canyon have become thicker resulting in accumulation of overspilled turbidites on the canyon flank and a decrease in the accumulation rate in MD3291 as a result of partial erosion by individual turbidity-current event. These more frequent and thick turbidity currents are interpreted as resulting from enhanced rainfall intensity. Moreover, compared to other source-to-sink systems, the turbidite occurrence in the flank of the Gaoping Canyon through the last glacial cycle may have been more strongly influenced by climatic changes due to short sediment storage/response times as results of

smaller drainage areas as well as a direct connection of canyon head and river mouth.

Acknowledgements

The authors would like to thank Ministry of Science and Technology, Taiwan (MOST) (grant number: MOST 104-2611-M-008-004) and Central Geological Survey, MOEA (grant number: 99-5226904000-04-02), Taipei, Taiwan, R.O.C. fund this research. Moreover, we also wish to thank Kuo-Yen Wei (National Taiwan University), Chih-Chieh Su (National Taiwan University), Yuan-Pin Chang (National Sun Yat-sen University), Tien-Nan Yang (CPC Corporation, Taiwan), James E. Hunt (National Oceanography Centre, Southampton), Michael Clare (National Oceanography Centre, Southampton) and Christopher J. Stevenson (University of Manchester) offer technical supports and helpful comments.

References

- Allen, P.A., 2008. From landscapes into geological history. *Nature* 451, 274–276.
- Bard, E., 1988. Correction of accelerator mass spectrometry ^{14}C ages measured in planktonic foraminifera: paleoceanographic implications. *Paleoceanography* 3, 635–645.
- Bernhardt, A., Hebbeln, D., Regenber, M., Lückge, A., Strecker, M.R., 2016. Shelf sediment transport by an undercurrent forces turbidity current activity during high sea level along the Chile continental margin. *Geology* 44 (4), 295–298.
- Blum, M.D., Hattier-Womack, J., 2009. Climate change, sea-level change, and fluvial sediment supply to deepwater depositional systems. In: Kneller, B., Martinsen, O.J., McCaffrey, B. (Eds.), *External Controls on Deep-water Depositional Systems Society for Sedimentary Geology, SEPM Special Publication*, pp. 15–39 (Tulsa, Oklahoma, USA).
- Bouma, A.H., 1962. *Sedimentology of Some Flysch Deposits: A Graphic Approach to Facies Interpretation*. Elsevier, Amsterdam (168 pp).
- Bourget, J., Zaragosi, S., Ellouz-Zimmermann, N., Mouchot, N., Garlan, T., Schneider, J.-L., Lanfumey, V., Lallemand, S., 2011. Turbidite system architecture and sedimentary processes along topographically complex slopes: the Makran convergent margin. *Sedimentology* 58, 376–406.
- Brushci, R., Bughi, S., Spinazzè, M., Torselletti, E., Vitali, L., 2006. Impact of debris flows and turbidity currents on seafloor structures. *Nor. J. Geol.* 86, 317–337.
- Carter, L., Milliman, J.D., Talling, P.J., Gavey, R., Wynn, R.B., 2012. Near-synchronous and delayed initiation of long run-out submarine sediment flows from a record-breaking river flood, offshore Taiwan. *Geophys. Res. Lett.* 39, L12603.
- Carter, L., Gavey, R., Talling, P.J., Liu, J.T., 2014. Insights into submarine geohazards from breaks in subsea telecommunication cables. *Oceanography* 27 (2), 58–67.
- Chang, Y.P., Wu, S.M., Wei, K.Y., Murayama, M., Kawahata, K., Chen, M.T., 2005. Foraminiferal oxygen isotope stratigraphy and high-resolution organic carbon, carbonate records from the Okinawa Trough (IMAGES MD012404 and ODP Site 1202). *Terr. Atmos. Ocean. Sci.* 16 (1), 57–73.
- Chen, H., Dadson, S., Chi, Y.G., 2006. Recent rainfall-induced landslides and debris flow in northern Taiwan. *Geomorphology* 77, 112–125.
- Chen, C.S., Chen, Y.L., Liu, C.L., Lin, P.L., Chen, W.C., 2007. Statistics of heavy rainfall occurrences in Taiwan. *Weather Forecast.* 22, 981–1002.
- Chiang, C.S., Yu, H.S., 2006. Morphotectonics and incision of the Kaoping submarine canyon, SW Taiwan orogenic wedge. *Geomorphology* 80, 199–213.
- Chiang, C.S., Yu, H.S., 2008. Evidence of hyperpycnal flows at the head of the meandering Kaoping Canyon off SW Taiwan. *Geo-Mar. Lett.* 28, 161–169.
- Clare, M.A., Talling, P.J., Challenor, P., Malgesini, G., Hunt, J.E., 2014. Distal turbidites reveal a common distribution for large ($> 0.1 \text{ km}^3$) submarine landslide recurrence. *Geology* 42 (3), 263–266.
- Clare, M.A., Talling, P.J., Hunt, J.E., 2015. Implications of reduced turbidity current and landslide activity for the Initial Eocene Thermal Maximum – evidence from two distal, deep-water sites. *Earth Planet. Sci. Lett.* 420, 102–115.
- Crookshanks, S., Gilbert, R., 2008. Continuous, diurnally fluctuating turbidity currents in Klane Lake, Yukon Territory. *Can. J. Earth Sci.* 45, 1123–1138.
- Curray, J.R., Emmel, F.J., Moore, D.G., 2003. The Bengal Fan: morphology, geometry, stratigraphy, history and processes. *Mar. Pet. Geol.* 19, 1191–1223.
- Dadson, S.J., Hovius, N., Chen, H., Dade, W.B., Hsieh, M.L., Willett, S.D., Hu, J.C., Horng, M.J., Chen, M.C., Stark, C.P., Lague, D., Lin, J.C., 2003. Links between erosion, runoff variability and seismicity in the Taiwan orogeny. *Nature* 426, 648–651.
- Droz, L., Bellaiche, G., 1985. Rhone deep-sea fan – morphostructure and growth-pattern. *AAPG Bull.* 69, 460–479.
- Ducassou, E., Migeon, S., Mulder, T., Murat, A., Capotondi, L., Bernasconi, S.M., Mascle, J., 2009. Evolution of the Nile deep-sea turbidite system during the Late Quaternary: influence of climate change on fan sedimentation. *Sedimentology* 56, 2061–2090.
- Fournier, L., Fauquembergue, K., Zaragosi, S., Zorzi, C., Malaizé, B., Bassinot, F., Jousain, R., Colin, C., Moreno, E., Leparmentier, F., 2016. The Bengal fan: external controls on the Holocene Active Channel turbidite activity. *The Holocene* 1–14.
- Galewsky, J., Stark, C.P., Dadson, S.J., Wu, C.C., Sobel, A.H., Horng, M.J., 2006. Tropical cyclone triggering of sediment discharge in Taiwan. *J. Geophys. Res.* 111, F03014.
- Gilbert, R., Crookshanks, S., Hodder, K., Spagnol, J., Stull, R., 2006. The record of an extreme flood in the sediments of montane Lake Lillooet, British Columbia: implications for paleo-environmental assessment. *J. Paleolimnol.* 37, 737–745.
- Goldfinger, C., Grijalva, K., Bürgmann, R., Morey, A.E., Johnson, J.E., Nelson, C.H., Gutiérrez-Pastor, J., Ericsson, A., Karabanov, E., Chaytor, J.D., Patton, J., Gràcia, E., 2008. Late Holocene rupture of the Northern San Andreas Fault and possible stress linkage to the Cascadia subduction zone. *Bull. Seismol. Soc. Am.* 98 (2), 861–889.
- Goldsmith, S.T., Carey, A.E., Lyons, W.B., Kao, S.J., Lee, T.Y., Che, J., 2008. Extreme storm events, landscape denudation, and carbon sequestration: typhoon Mindulle, Choushui River, Taiwan. *Geology* 36, 483–486.
- Hsieh, M.L., Chyi, S.J., 2010. Late Quaternary mass-wasting records and formation of fan terraces in the Chen-yeo-lan and Lao-nung catchments, central-southern Taiwan. *Quat. Sci. Rev.* 29, 1399–1418.
- Hsu, S.K., Kuo, J., Lo, C.L., Tsai, C.H., Doo, W.B., Ku, C.Y., Sibuet, J.C., 2008. Turbidity currents, submarine landslides and the 2006 Pingtung earthquake off SW Taiwan. *Terr. Atmos. Ocean. Sci.* 19, 767–772.
- Hsu, R.T., Liu, J.T., Su, C.C., Kao, S.J., Chen, S.N., Kuo, F.H., Huang, J.C., 2014. On the links between a river's hyperpycnal plume and marine benthic nepheloid layer in the wake of a typhoon. *Prog. Oceanogr.* 127, 62–73.
- Huh, C.A., Lin, H.L., Lin, S., Huang, Y.W., 2009. Modern accumulation rates and a budget of sediment off the Gaoping (Kaoping) River, SW Taiwan: a tidal and flood dominated depositional environment around a submarine canyon. *J. Mar. Syst.* 76, 405–416.
- Ingersoll, R.V., Dickinson, W.R., Graham, S.A., 2003. Remnant-ocean submarine fans: Largest sedimentary systems on earth. In: *Special Papers — Geological Society of America*, pp. 191–208.
- Kao, S.J., Dai, M., Selvaraj, K., Zhai, W., Cai, P., Chen, S.-N., Yang, J.-Y., Liu, J.T., Liu, C.-C., Syvitski, J.P.M., 2010. Cyclone-driven deep sea injection of freshwater and heat by hyperpycnal flow in the subtropics. *Geophys. Res. Lett.* 37, L21702.
- Lambeck, K., Rouby, H., Purcell, A., Sun, Y., Sambridge, M., 2014. Sea level and global ice volumes from the Last Glacial Maximum to the Holocene. *PNAS* 111 (43), 15296–15303.
- Lambert, A., Hsu, K.J., 1979. Non-annual cycles of varve-like sedimentation in Walensee, Switzerland. *Sedimentology* 26, 453–461.
- Lebreiro, S.M., Voelker, A.H.L., Vizcaino, A., Abrantes, F.G., Alt-Epping, U., Jung, S., Thouveny, N., Gracia, E., 2009. Sediment instability on the Portuguese continental margin under abrupt glacial climate changes (last 60 kyr). *Quat. Sci. Rev.* 28, 3211–3223.
- Lee, C.Y., Liew, P.M., 2010. Late Quaternary vegetation and climate changes inferred from a pollen record of Dongyuan Lake in southern Taiwan. *Palaeogeogr. Palaeoclimatol. Palaeoecol.* 287, 58–66.
- Lee, C.Y., Liew, P.M., Lee, T.Q., 2010. Pollen records from southern Taiwan: implications for East Asian summer monsoon variation during the Holocene. *The Holocene* 20, 81–89.
- Lin, A.T., Liu, C.S., Lin, C.C., Schnurle, P., Chen, G.Y., Liao, W.Z., Teng, L.S., Chuang, H.J., Wu, M.S., 2008. Tectonic features associated with the overriding of an accretionary wedge on top of a rifted continental margin: an example from Taiwan. *Mar. Geol.* 255, 186–203.
- Liu, J.T., Lin, H.L., 2004. Sediment dynamics in a submarine canyon: a case of river–sea interaction. *Mar. Geol.* 207 (1–4), 55–81.
- Liu, C.S., Lundberg, N., Reed, D.L., Huang, T.L., 1993. Morphological and seismic characteristics of the Kaoping submarine canyon. *Mar. Geol.* 111, 93–108.
- Liu, J.T., Liu, K.J., Huang, J.C., 2002. The effect of a submarine canyon on the river sediment dispersal and inner shelf sediment movement in southern Taiwan. *Mar. Geol.* 181, 357–386.
- Liu, Z., Colin, C., Trentesaux, A., Blamart, D., Bassinot, F., Siani, G., Sicre, M.A., 2004. Erosional history of the eastern Tibetan Plateau over the past 190 kyr: clay mineralogical and geochemical investigations from the southwestern South China Sea. *Mar. Geol.* 209, 1–18.
- Liu, J.T., Lin, H.L., Hung, J.J., 2006. A submarine canyon conduit under typhoon conditions off Southern Taiwan. *Deep-Sea Res.* I 53, 223–240.
- Liu, T.J., Hung, J.J., Lin, H.L., Huh, C.A., Lee, C.L., Hsu, R.T., Huang, Y.W., Chu, J.C., 2009. From suspended particles to strata: the fate of terrestrial substances in the Gaoping (Kaoping) submarine canyon. *J. Mar. Syst.* 76, 417–432.
- Liu, Z., Colin, C., Li, X., Zhao, Y., Tuo, S., Chen, Z., Siringan, F.P., Liu, J.T., Huang, C.-Y., You, C.-F., Huang, K.-F., 2010a. Clay mineral distribution in surface sediments of the northeastern South China Sea and surrounding fluvial drainage basins: source and transport. *Mar. Geol.* 277, 48–60.
- Liu, J.T., Wang, Y.H., Lee, I.H., Hsu, R.T., 2010b. Quantifying tidal signatures of the benthic nepheloid layer in Gaoping Submarine Canyon in Southern Taiwan. *Mar. Geol.* 271, 119–130.
- Liu, J.T., Wang, Y.H., Yang, R.J., Hsu, R.T., Kao, S.J., Lin, H.L., Kuo, F.H., 2012. Cyclone-induced hyperpycnal turbidity currents in a submarine canyon. *J. Geophys. Res.* 117, C04033.
- Liu, J.T., Kao, S.J., Huh, C.A., Hung, C.C., 2013. Gravity flows associated with flood events and carbon burial: Taiwan as instructional source area. *Annu. Rev. Mar. Sci.* 5 (57–68), 12.1–12.22.
- Liu, T.J., Hsu, R.T., Hung, J.J., Chang, Y.P., Wang, Y.H., Rendle-Bühning, R.H., Lee, C.L., Huh, C.A., Yang, R.J., 2016. From the highest to the deepest: the Gaoping River-Gaoping Submarine dispersal system. *Earth Sci. Rev.* 153, 274–300.
- Mauffrey, M.A., Urgeles, R., Berné, S., Canning, J., 2017. Development of submarine canyons after the Mid-Pleistocene Transition on the Ebro margin, NW Mediterranean: the role of fluvial connections. *Quat. Sci. Rev.* 158, 77–93.
- Milliman, J.D., Syvitski, P.M., 1992. Geomorphic/tectonic control of sediment discharge to the ocean: the importance of small mountainous rivers. *J. Geol.* 100 (5), 525–544.
- Nydal, R., Lövsæth, 1965. Distribution of radiocarbon from nuclear tests. *Nature* 206, 1029–1031.
- Piper, D.J.W., Normark, W.R., 2009. Processes that initiate turbidity currents and their

- influence on turbidites: a marine geology perspective. *J. Sediment. Res.* 79, 347–362.
- Poñt, D., Simonnet, J.P., Walter, A.V., 2002. Medium-term changes in suspended sediment delivery to the ocean: consequences of catchment heterogeneity and river management (Rhône River, France). *Estuar. Coast. Shelf Sci.* 54, 1–18.
- dos Reis, A.T., Gorini, C., Mauffret, A., 2005. Implications of salt-sediment interactions on the architecture of the Gulf of Lions deep-water sedimentary systems – western Mediterranean Sea. *Mar. Pet. Geol.* 22, 713–746.
- Selvaraj, K., Lee, T.Y., Yang, J.Y.T., Canuel, E.A., Huang, J.C., Dai, M., Liu, J.T., Kao, S.J., 2015. Stable isotopic and biomarker evidence of terrigenous organic matter export to the deep sea during tropical storms. *Mar. Geol.* 364, 32–42.
- Sparkes, R.B., Lin, I.T., Hovius, N., Galy, A., Liu, J.T., Xu, X.M., Yang, R., 2015. Redistribution of multi-phase particulate organic carbon in a marine shelf and canyon system during an exceptional river flood: effects of Typhoon Morakot on the Gaoping River-Canyon system. *Mar. Geol.* 363, 191–201.
- Stevenson, C.J., Talling, P.J., Masson, D.G., Sumner, E.J., Frenz, M., Wynn, R.B., 2014. The spatial and temporal distribution of grain-size breaks in turbidites. *Sedimentology* 61, 1120–1156.
- Stow, D.A.V., Piper, D.J.W., 1984. Deep-water fine-grained sediments: facies models. In: Stow, D.A.V., Piper, D.J.W. (Eds.), *Fine-grained Sediments: Deep-water Processes and Facies*. Special Publications, Geological Society of London 14pp. 611–645.
- Su, C.C., Tseng, J.Y., Hsu, H.-H., Chiang, C.S., Yu, H.S., Lin, S., Liu, J.T., 2012. Records of submarine natural hazards off SW Taiwan. In: *Natural Hazards in the Asia-Pacific Region*. Special Publications, Geology Society of London 361pp. 41–60.
- Talling, P.J., 2014. On the triggers, resulting flow types and frequencies of subaqueous sediment density flows in different settings. *Mar. Geol.* 352, 155–182.
- Tombo, S.L., Dennielou, B., Berné, Bassetti, M.A., Toucanne, S., Jorry, S.J., Jouet, G., Fontanier, C., 2015. Sea-level control on turbidite activity in the Rhône canyon and the upper fan during the Last Glacial Maximum and early deglacial. *Sediment. Geol.* 323, 148–166.
- Umeda, M., Yokoyama, K., Ishikawa, T., 2006. Observation and simulation of floodwater intrusion and sedimentation in the Shichikashuku Reservoir. *J. Hydraul. Eng.* 132, 881–891.
- Vorren, T.O., Laberg, J.S., Blaume, F., Dowdeswell, J.A., Kenyon, N.H., Mienert, J., Rumohr, J., Werner, F., 1998. The Norwegian-Greenland sea continental margins: morphology and late Quaternary sedimentary processes and environment. *Quat. Sci. Rev.* 17 (1–3), 173–302.
- Walsh, J.P., Nittrouer, C.A., 2009. Understanding fine-grained river-sediment dispersal on continental margins. *Mar. Geol.* 263 (1), 34–45.
- Wang, C.H., Li, L.A., Liu, W.C., 1994. Some characteristics of the precipitation in Taiwan. In: Peng, C.-I., Chou, C.H. (Eds.), *Biodiversity and Terrestrial Ecosystem*. Academia Sinica Monograph Series No. 14 Institute of Botany, Taipei, pp. 343–354.
- Weaver, P.P.E., Wynn, R.B., Kenyon, N.H., Evans, J., 2000. Continental margin sedimentation, with special reference to the north-east Atlantic margin. *Sedimentology* 47, 239–256.
- Weber, M.E., Wiedicke, M.H., Kudrass, H.R., Hübscher, C., Erlenkeuser, H., 1997. Active growth of the Bengal Fan during sea-level rise and highstand. *Geology* 25 (4), 315–318.
- Yang, T.-N., Lee, T.-Q., Meyers, P.A., Song, S.R., Kao, S.-J., Löwemark, L., Chen, R.-F., Chen, H.-F., Wei, K.-Y., Fan, C.-W., Shiau, L.-J., Chiang, H.-W., Chen, Y.-G., Chen, M.-T., 2011. Variations in monsoonal rainfall over the last 21 kyr inferred from sedimentary organic matter in Tung-Yuan Pond, southern Taiwan. *Quat. Sci. Rev.* 30, 3413–3422.
- Yu, H.S., Chiang, C.S., Shen, S.M., 2009. Tectonically active sediment dispersal system in SW Taiwan margin with emphasis on the Gaoping (Kaoping) Submarine Canyon. *J. Mar. Syst.* 76, 369–382.